International Journal of Disaster Risk Reduction 31 (2018) 76–84

Contents lists available at ScienceDirect

International Journal of Disaster Risk Reduction

journal homepage: www.elsevier.com/locate/ijdrr

Synthetic building damage scenarios using empirical fragility functions: A case study of the 2016 Kumamoto earthquake

Luis Moya[a,*], Erick Mas[a], Shunichi Koshimura[a], Fumio Yamazaki[b]

[a] International Research Institute of Disaster Science, Tohoku University, Aoba 468-1-E301, Aramaki, Aoba-ku, Sendai 980-0845, Japan
[b] Department of Urban Environment System, Chiba University, Chiba 263-8522, Japan

ARTICLE INFO

Keywords:
Synthetic building damage scenario
The 2016 Kumamoto earthquake
Fragility curves

ABSTRACT

A methodology to create synthetic earthquake-induced building damage states for urban areas in Japan under specific earthquake events is presented in this paper. The methodology is based on empirical fragility curves for Japanese buildings, the building database of the study area and the strong motion magnitude spatial distribution. A stochastic approach was then used to allocate damage states to buildings. The synthetic building damage scenario is intended to be used as a platform for performing computational simulations of evacuation and relief distribution under multiple damage scenarios. The methodology is applied to an area within Mashiki town, Kumamoto Prefecture, which was affected by the Mw 7.0 2016 Kumamoto earthquake. The comparison of the synthetic buildings damage scenario with the surveyed data inventory shows good agreement in terms of the aggregate statistics.

1. Introduction

The assessment of multiple consequences in the aftermath of a large-scale earthquake constitutes a key step for decision-making and effective emergency response. It is important to point out that direct earthquake damage to buildings constitutes a small fraction of the total economic loss, which includes human casualties, loss of revenue and market, disruption of transportation and communication, etc. The methods to estimate building damage are classified in two groups [1]: (1) using empirical observations, based on ground motion parameters such as the Modified Mercalli intensity (MMI), peak ground acceleration (PGA), and peak ground velocity (PGV); and (2) using nonlinear models of structural response, based on spectral acceleration. Empirical methods rely on observations of the relationship between damage and ground motion. In the early stage, when strong-motion instrumentation was not available, the MMI was used [2,3]. With the advent of the strong-motion instrumentation, parameters like PGA or PGV were employed [4,5]. Whitman et al. [3] collected data on the damage caused by the 1971 San Fernando earthquake and presented statistical damage information. Yamazaki and Murao [4] and Horie et al. [6] proposed fragility functions for Japanese buildings based on building inventory, damage data, and the spatial distribution of strong motion during the 1995 Kobe, Japan, earthquake. Regarding the estimation of building damage from analytical methods, the building is modeled and a nonlinear analysis is performed using a family of strong motions. Then, the relation between the nonlinear structural response and a measure of the strong-motion is defined. The building can be modeled with different level of complexity, from a single degree of freedom (SDOF) to a multiple degrees of freedom (MDOF). Several methods for building damage models using nonlinear analysis have been proposed, such as capacity spectrum method [7] and displacement coefficient method [8]. Building damage functions is ubiquitous in all the frameworks of seismic risk analysis, such as Hazus [9–11] and Performance-based earthquake engineering (PBEE) [12–15]. Actually, the assessment of seismic risk requires the building damage models to be defined as a distribution of damage ratio given the strong-motion parameter. A lognormal distribution is the most common distribution used for building damage functions [4,16–18].

This paper focuses on the development of synthetic earthquake-induced building damage scenarios, hereafter referred as EBDS, based on empirical building damage functions. The synthetic damage state for each building does not necessary corresponds to the true damage state. However, the synthetic dataset will be statistically consistent with the aggregate values. A first question is as follows: What is the purpose of generating synthetic EBDS? In recent years, studies have been exploring the complex space-time social dynamics involved during a disaster event by mean of modeling and simulation. For instance, Mas et al. [19] identified bottlenecks and congested streets during the 2011 Great East Japan Earthquake based on an evacuation simulation using agent-based modeling (ABM). However, the effect of the damaged buildings was not

* Corresponding author.
E-mail address: lmoyah@irides.tohoku.ac.jp (L. Moya).

https://doi.org/10.1016/j.ijdrr.2018.04.016
Received 26 October 2017; Received in revised form 22 March 2018; Accepted 17 April 2018
Available online 24 April 2018

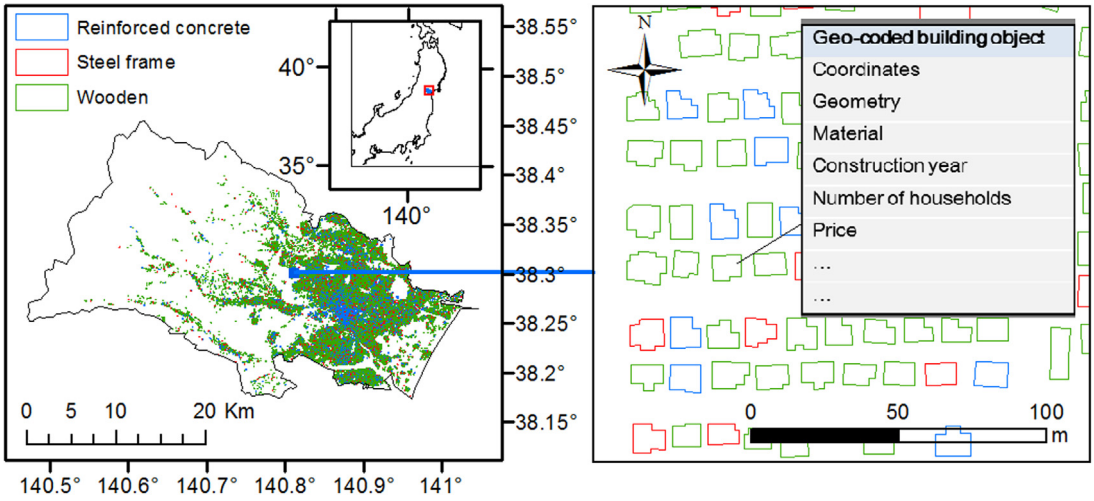

Fig. 1. Geocoded building database of Sendai city, Japan.

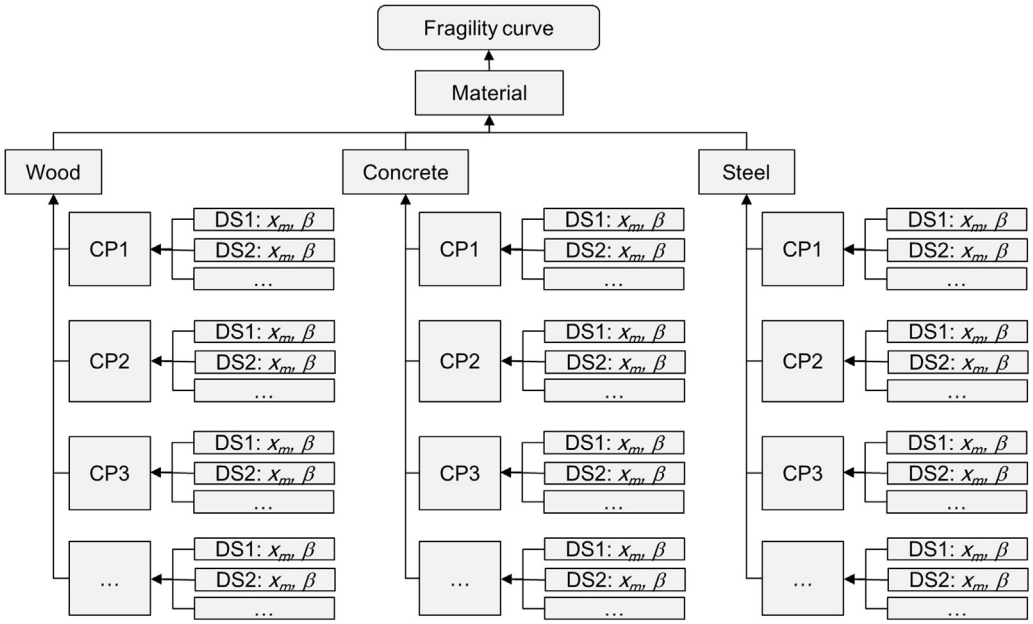

Fig. 2. Fragility curve flowchart (CP: construction period; DS: damage state).

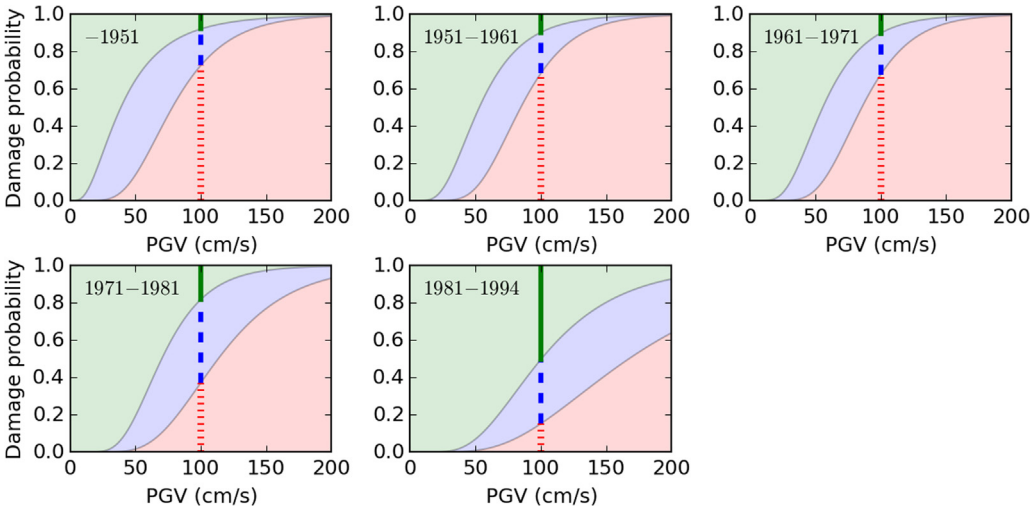

Fig. 3. Empirical fragility curves for Japanese wooden buildings proposed by Yamazaki and Murao (2000).

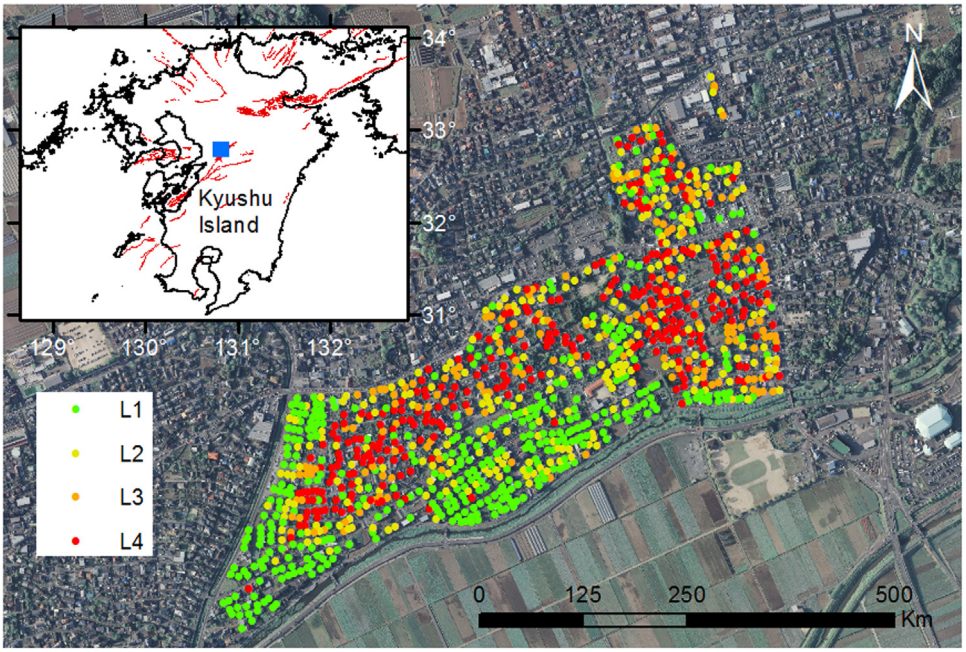

Fig. 4. Surveyed building damage. L1: Low/no damage; L2: Moderate damage; L3: Leaning buildings; L4: Collapsed buildings.

considered. Agent-based modeling (ABM) is a bottom-up approach in which each agent is an individual part of a system. Under particular rules, according to their role in the system, an agent is modeled as an autonomous decision-making entity [20]. Das and Hanaoka [21] used ABM for resource allocation in various zones after a large-scale disaster, where the Great East Japan Earthquake and Tsunami was used as a case study. Thus, the damage scenario was a fixed input. Nejat and Damnjanovic [22] evaluated the reconstruction process of an affected area by modeling the dynamic behavior of homeowners. In the aforementioned study, the damage pattern to each property was assumed to be proportional to its distance from a focal point; that is, a deterministic approach. The studies mentioned previously evidence a lack of a versatile procedure that can provide a consistent building damage scenario. The method presented here is intended to help experts on modeling and simulation to create building damage scenarios using a stochastic approach. This manuscript is not a substitute for understanding the fundamental concepts behind damage models. We estimated building damage scenarios in Mashiki town using the spatial distribution of PGV during the 2016 Kumamoto earthquake and contrast the result with surveyed building damage inventory.

2. Methodology

The EBDS is estimated by retrieving the ground motion parameters at the location of the geocoded building database and allocating a damage state based on fragility curves. For the implementation of this methodology, a higher-level programming language was preferred. Python provides an object-oriented dynamic programming environment and can be easily adjusted to specific needs. Additionally, Python comes with extensive and freely available scientific libraries. For our purposes, the Geospatial Data Abstraction Library (GDAL) is used to read and manipulate the geocoded building inventory dataset and to retrieve the ground motion in a raster data format. With the aid of GDAL, our framework directly interacts with the geocoded dataset and creates the synthetic EBDS in a geographic information system (GIS). Moreover, the Numpy library is used to manipulate arrays in the numerical work. Further details for the implementation of the synthetic EBDS are presented in the following section.

2.1. Building inventory

This section describes the geodatabase model designed to store the building inventory. The building inventory was provided by the local government and is stored in the shapefile (.shp) spatial data format [23] in which each building comprises building footprint geometry and attributes. The building footprint is stored as a shape comprising a set of vector coordinates. The attributes of each building include the construction year, number of floors, building construction type, number of households, and number of people. Fig. 1 shows the building distribution of Sendai city, Japan.

2.2. Earthquake scenario

The National Research Institute for Earth Science and Disaster Prevention (NIED) operates the two biggest strong motion networks in Japan: the Kyoshin Network (K-NET) and the Kiban-Kyoshin Network (KiK-net) [24]. K-NET consists of more than 1000 stations installed on the ground surface and distributed uniformly over the Japan's territory. KiK-net consist of approximately 700 stations, each of which is equipped with two accelerometers, one installed in a borehole and another on the ground surface.

The projection of ground motion in a map view for an earthquake event is provided by QuiQuake [25]. QuiQuake generates two types of strong motion maps: QuickMap and QuakeMap. For our framework, the QuakeMap output is used. QuakeMap uses the strong motion records from K-NET and KiK-net to calculate the ground motion parameters, PGA, PGV and I_{JMA}, at the surface of the stations. Then, using amplification factors, the ground motion parameters at the rock level are calculated. A Simple Kriging interpolation method with a trend component is then applied to estimate the spatial distribution of the ground motion parameters at the base-rock level. Finally, the ground motion parameters at the surface are calculated using the amplification factors. Further information regarding the QuiQuake framework can be found in [25]. For the generation of synthetic EBDS, a program that uses QuakeMap to find the ground motion parameters at sites of interest was implemented. The program is employed to extract the PGV at building locations. The program verifies whether both the building database and the QuakeMap have the same spatial coordinate system and changes the coordinate system if necessary.

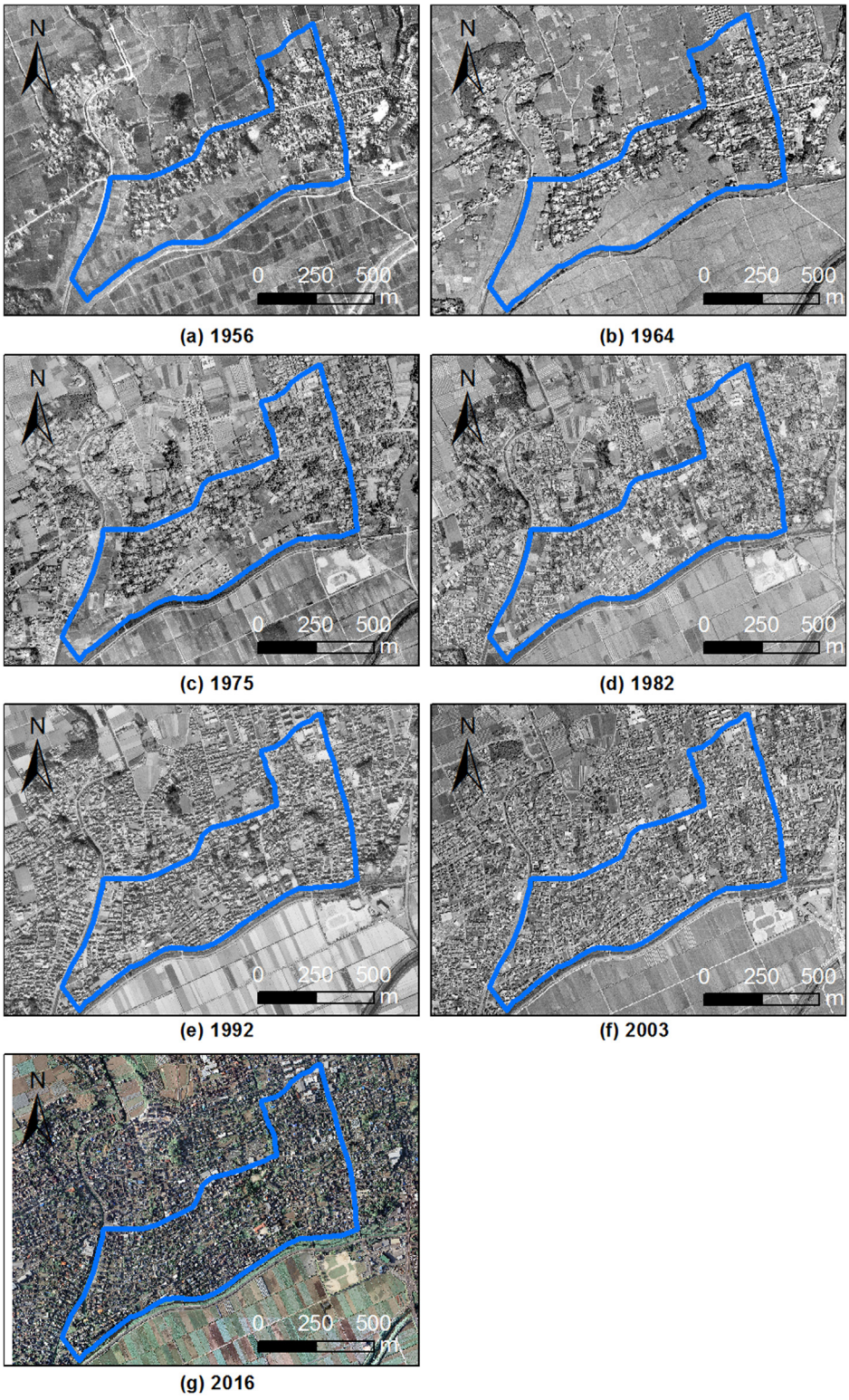

Fig. 5. Aerial photos of the study area taken at different periods. The blue polygon shows the area where the building damage survey were performed.

2.3. Fragility curves

This module stores the fragility functions used for the synthetic EBDS. A fragility function provides the likelihood that an element will reach or exceed a certain level of damage (DM) under a given engineering demand parameter (EDP) [17]. In general, for seismic risk analysis, fragility curves are expressed as a logarithmic cumulative distribution function:

$$F_{dm}(edp) = P[DM \geq dm | EDP = edp] \quad (1)$$

$$F_{dm}(edp) = \Phi\left(\frac{\ln(edp/x_m)}{\beta}\right) \quad (2)$$

where Φ refers to the normal cumulative distribution function, x_m denotes the median value of the distribution, β is the logarithmic standard deviation, edp denotes a particular value of EDP, and dm is a particular

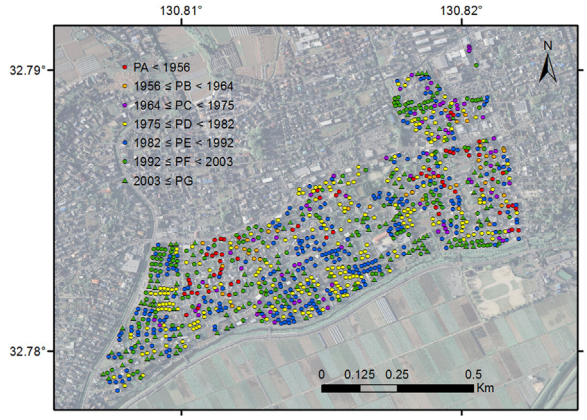

Fig. 6. Construction period of the buildings according to the aerial photos.

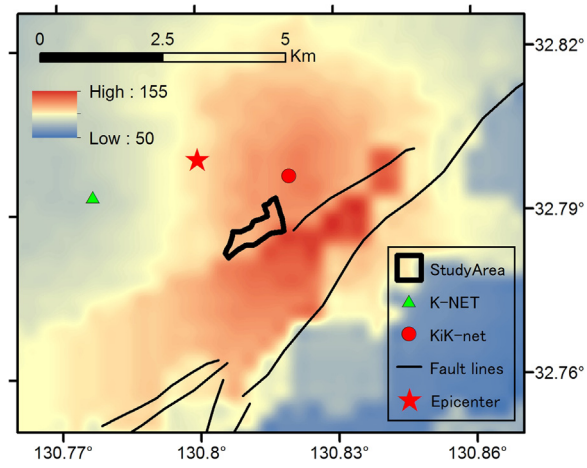

Fig. 7. Spatial distribution of the PGV provided by QuakeMap. The black polygon shows the location of the study area. The triangle and circle marks denotes the accelerometers from K-NET and KiK-net, respectively.

value of DM. When a set of fragility curves for different damage states are available, the probability that a building is in damage state dm given $EDP = edp$ is:

$$\begin{aligned} P[DM= \ dm|EDP = edp] &= 1 - F_1(edp), \quad dm = 0 \\ &= F_{dm}(edp) - F_{d+1}(edp), \quad 1 \le dm < N \\ &= F_{dm}(edp), \quad dm = N \end{aligned} \tag{3}$$

where N denotes the number of possible damage states in addition to the non-damage state ($d = 0$). The empirical fragility functions proposed by Yamazaki and Murao [4] were employed for the synthetic EBDS model. The reason behind this decision is that these functions are often used in earthquake damage assessment in Japan by the Bureau of Urban Development of the Tokyo Metropolitan Government [26]. "No/slight", "Moderate", and "Heavy" damage states were adopted. Here, the PGV is used as the EDP. Yamazaki and Murao [4] used the building damage inventory collected after the 1995 Hyogoken-Nanbu (Kobe) earthquake and proposed a set of empirical fragility functions for four structural types, namely, wood-frame, reinforced concrete, steel, and light-gauge steel, as well as for 5 different construction periods, namely, before 1951, 1951–1961, 1961–1971, 1971–1981, and 1981–1994. For buildings constructed after the Kobe earthquake, a modification of the empirical fragility curves based on the building damage inventory collected after the 2007 Niigata-Ken Chuetsu-Oki Earthquake is employed [27].

Within the synthetic EBDS model, the framework uses the correct set of fragility curves according to each building typology (i.e., building construction type and construction year) stored in the building inventory. First, the PGV is extracted from the QuakeMap at the building location. Then, the empirical fragility curves are used to estimate the probability of each damage state from Eq. (3). Fig. 2 shows the arrangement of the module that stores the fragility curves parameters.

2.4. Generation of synthetic EBDS

The proposed method allocates a damage state to each building using the empirical fragility functions published in previous studies. The use of fragility functions to simulate damage states have been applied before [28]. The main constraint is to minimize the error in the percent of damaged buildings. With that purpose, a random number generator technique with a given distribution was chosen; that is, each building damage state is associated to a discrete range of numbers:

$$DM = [0, 1, 2] = [\text{“}non/slight\text{”}, \text{“}moderate\text{”}, \text{“}heavy\text{”}] \tag{4}$$

Then, these discrete numbers are generated randomly using a consistent distribution. Here, the distribution of the discrete numbers is calculated from Eq. (3):

$$p = \begin{pmatrix} p_0 \\ p_1 \\ p_2 \end{pmatrix} = \begin{pmatrix} P[DM = 0|PGV = pgv] \\ P[DM = 1|PGV = pgv] \\ P[DM = 2|PGV = pgv] \end{pmatrix} \tag{5}$$

Therefore, the random selection is performed using a distribution that represents the probabilities for each damage state. For a better comprehension of the use of fragility curves, Fig. 3 depicts the fragility curves proposed by [4] for wood buildings. A vertical line is drawn at a PGV = 100 cm/s, in which the length of the solid, dashed, and dotted segments depict the probability of no/slight, moderate, and heavy damage states, respectively. These values are used to generate the random numbers. The effect of the construction period on the probability of damage states can be seen. For instance, for the group of wood buildings with the same PGV, the number of old buildings with heavy

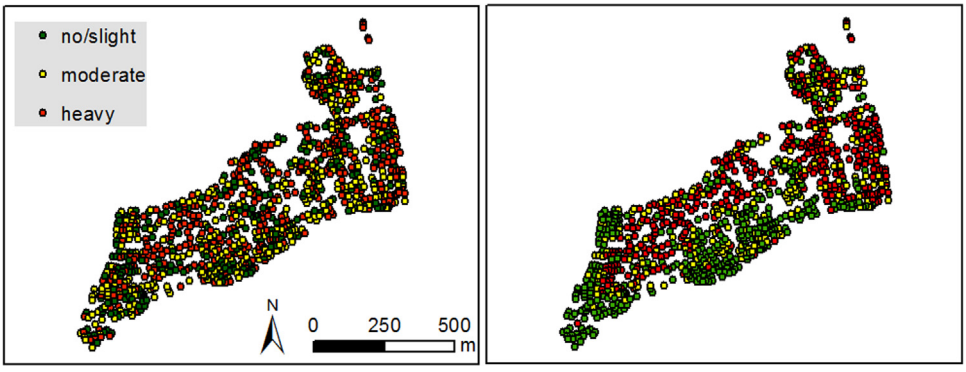

Fig. 8. Left: An instance of a synthetic EBDS. Right: The actual EBDS from field survey.

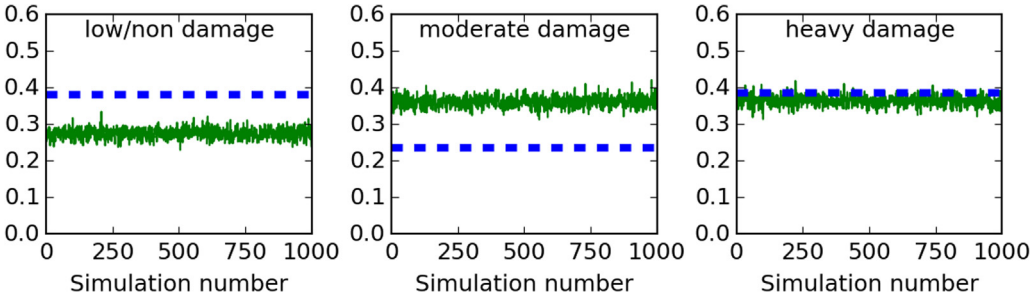

Fig. 9. Comparison of damage ratio between synthetic building damage (Case I) and actual damage ratio.

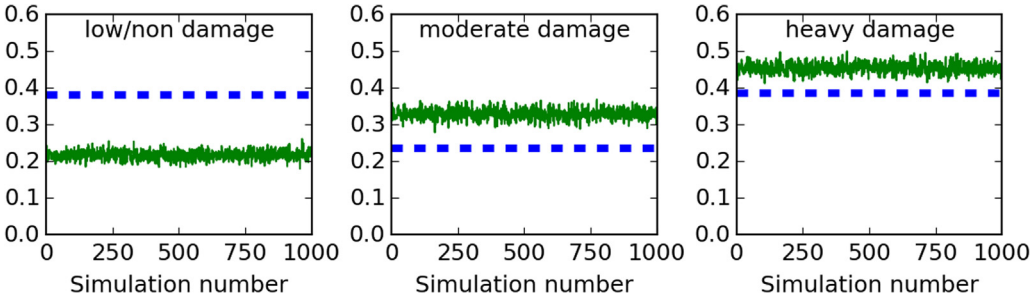

Fig. 10. Comparison of damage ratio between synthetic building damage (Case II) and actual damage ratio.

Table 1
Actual damage state ratios of the study area and the average and standard deviation of the damage state ratios of the synthetic data.

Damage state	Actual ratio	Case I	Case II
Low	0.380	0.274 ± 0.014	0.217 ± 0.012
Moderate	0.235	0.362 ± 0.015	0.329 ± 0.014
Heavy	0.385	0.364 ± 0.014	0.454 ± 0.014

damage will be larger than that for newer buildings. Furthermore, for a group of buildings within the same construction period, when the demand (PGV) increases, the probability of experiencing heavy damage increases, while the probability of slight/no damage decreases.

3. Experimental results and analysis

In order to test the application and evaluate its performance, the 2016 Mw 7.0 Kumamoto earthquake is selected as a case study. On 14 April 2016, a Mw 6.2 earthquake struck Kumamoto Prefecture, Japan, at 21:26 JST. The epicenter was located at the end of the Hinagu fault at a shallow depth. After approximately 28 h (at 01:25 JST on 16 April 2016), another earthquake of Mw 7.0 struck the same area. The epicenter occurred at the Futagawa fault near the Hinagu fault. The Futagawa and Hinagu faults are well-known active faults on Kyushu island, Japan. The first and second events were designated as the foreshock and mainshock, respectively. With 340 aftershocks larger than Mw 3.5 up to April 2017, the Kumamoto earthquake is the inland event that has produced the largest number of aftershock in Japan [29]. The city of Mashiki, with a population of approximately 33,000, was the most affected. Buildings, bridges and lifelines were severely affected. According to the Cabinet Office of Japan, a total of 8697 houses collapsed and 228 casualties occurred as of April 13, 2017 [30].

Several research teams surveyed the affected area. Fig. 4 shows the surveyed building damage states performed by Yamada et al. [31,32]. The survey was performed within one of the most affected areas in Mashiki town. Four levels of damage were selected in the survey: no/low damage (L1), moderate damage (L2), inclined building (L3), and collapsed building (L4). The building material was also recorded during the survey as well. Additionally, Yamada et al. [31] extracted the buildings that had collapsed due to the foreshock using aerial photos. For our purposes, the buildings affected by the foreshock were filtered, and the inclined and collapsed buildings were merged to represent the heavily damaged buildings.

Unfortunately, there was no information regarding to the construction period of the buildings in the affected area, and this information is necessary for the use of empirical fragility curves. Here, we set up construction periods based on a set of aerial photos taken in the years of 1956, 1964, 1975, 1982, 1992, 2003, and 2016 (Fig. 5). The aerial photos were provided by the Geospatial Information Authority of Japan (GSI) [33] and were chosen as the best possible matches for the construction periods from which the empirical fragility curves were constructed. Before extracting the construction period of each buildings, a corregistration of the aerial images was necessary. For that purpose, the 2016 aerial photo, which was georeferenced, was used as a reference image to align the other aerial photos. Common features, such as the Akitsu river and main roads, were used for the alignment. Fig. 6 shows the construction period according to the aerial photos.

Fig. 7 shows the spatial distribution of the PGV provided by QuakeMap. In this study, we analyze wooden buildings only because the number of reinforced concrete and steel buildings within the study areas was almost negligible. A total of 972 wooden buildings were used. The empirical fragility curves of Yamazaki and Murao [4] were applied for buildings with construction year earlier than 1994; otherwise, the modification of Nagao and Yamazaki [27] was employed. As mentioned above, a construction period based on aerial photos was associated to each building (Fig. 6). However, there was not a perfect match between the construction periods and the fragility curves (Fig. 3). Therefore, two sets of fragility functions corresponding to two consecutive construction periods were associated to some buildings.

After gathering all the required inputs, two sets of simulations were performed. In the first case (case I), the latest associated construction period of the buildings was used. The oldest construction period associated to each building was used in the second case (case II). For each set, 1000 simulations were carried out. Fig. 8a illustrates a simulation from case I. As mentioned above, the synthetic damage states differ from the real damage (Fig. 8b). Recall that the synthetic data were built from the empirical fragility curves, which represent only aggregate values. Regarding to the aggregate values, Figs. 9 shows the damage

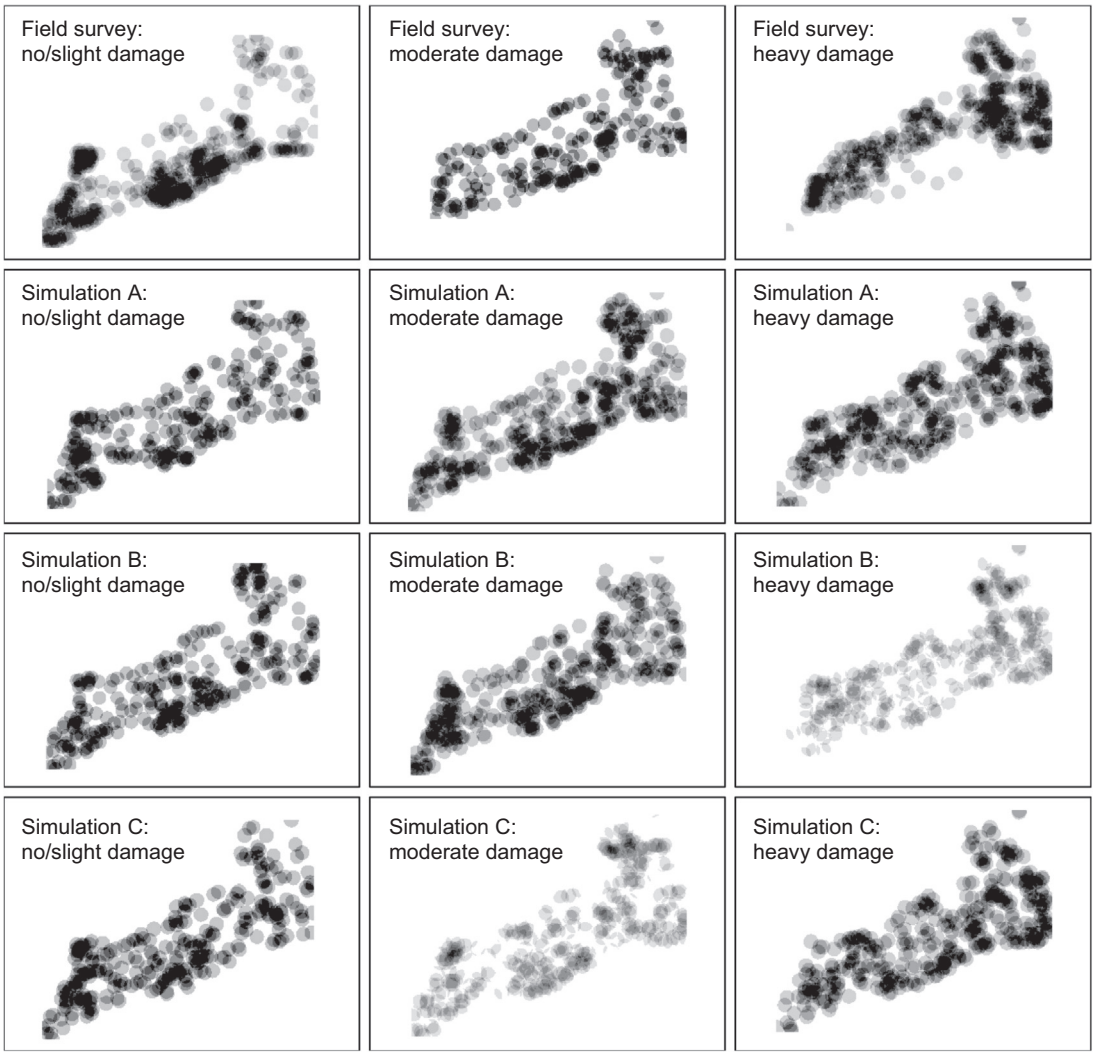

Fig. 11. Comparison of density of buildings between field data survey and three synthetic damage scenarios for each damage state. The black areas depicts the highest density of buildings.

ratio of the study area calculated from each simulation (solid green line) of the first set and the actual damage ratio (dashed blue line). Similar results from case II are shown in Fig. 10. It is observed that the synthetic damage ratios oscillate around a constant value. This pattern demonstrates that the creation of random damage states using a defined distribution keeps the aggregate values nearly constant. The average and standard deviation of the synthetic damage states ratios are depicted in Table 1. The largest standard deviation observed is 1.5%, which is fairly low. Another issue is the observed difference between the actual and the synthetic damage states ratios. Remember that the synthetic damage states are created based on aggregate values of previous events. The best agreement is in the heavy damage ratios, with differences of 2% and 7% for case I and case II, respectively. If the building construction year were available, the difference between the real and the synthetic damage states would be somewhere in the middle of these two cases. The synthetic moderate damage ratio is overestimated by 13% and 7% for case I and case II, respectively. Thus, the estimation of buildings with a moderate damage state is conservative for the Kumamoto earthquake. The largest discrepancies are observed in the low/non damage ratio, with differences of 11% and 16% for case I and case II, respectively, with underestimations in both cases. Overall, the results are conservatively desirable, with slight overestimations for moderate and heavy damage states and underestimation for slow/non damage state. The opposite results would be undesirable.

In order to evaluate the spatial distribution of the synthetic EBDS, the density of buildings for each damage state was calculated. Following the same procedure, the density of buildings of the truth data was calculated as well. Fig. 11 shows the density of buildings for three synthetic scenarios and the truth data. It was observed that the synthetic EBDS produced some sparsity in the spatial distribution. However, the areas where they are clustering show a similar trend as the truth data. For instance, buildings with no/slight damage are clustering in the southwest and the center of the area of the study area. On the other hand, buildings with heavy damage are clustering in part of the center and the northwest.

4. Discussion and conclusions

In this paper, the implementation of a framework to create synthetic damage scenarios using empirical fragility functions and GIS is briefly described. The required inputs for the model are presented in detail. The procedure is based on stochastic simulations to create several different damage scenarios while guaranteeing fairly accurate aggregate values of the damage states, that is, the damage states ratios. Then, the framework was tested for the 2016 Mw 7.0 Kumamoto earthquake. The damage state ratios were evaluated by comparing them with the actual damage ratio of a surveyed area, and a good agreement was observed. From the comparison, the number of buildings with heavy and

moderate damage states generated in the synthetic scenarios were slightly larger than the actual amount; meanwhile, the number of buildings with slight damage/non-damaged states was lower in the synthetic scenarios. Thus, the synthetic scenarios are conservative, which is desirable when a microscale building damage scenario estimation is required.

Several factors might contribute to the difference between the synthetic and the actual damage state ratios. For instance, the representation of the demand is simplified to one parameter (PGV). However, other factors, such as the predominant period of the strong motion, are sometimes important. Another issue is the structural system; although wooden buildings in Japan are constructed using the same earthquake building code, some differences in their configuration are observed in different regions. For example, buildings in the north are built with heavier and stiffer roof systems to withstand snow. Therefore, buildings from different regions may have different performances.

In the proposed method, the peak ground motion was obtained from dense networks. However, the peak ground motion can be estimated using ground-motion prediction equations (GMPE), which can be used in the absence of ground-motion networks or when the effects of future earthquakes is desired to be evaluated. There is an extensive literature that deals with GMPE as well as the number of the proposed models. It is thus important to have a criterion in the selection of appropriate GMPE. A modern treatment with a number of suggestions to select a GMPE can be found in [34]

It is important to point out that the representation of an earthquake event by the peak ground motion has limitations in representing the complexities of an event. In fact, in the case of the 2016 Kumamoto earthquake, a significant foreshock occurred approximately 28 h before the mainshock. The uncertainties product of that foreshock has the same nature of the following issues: (1) During the strong-motion, a building might experience several oscillations larger than the yielding point and this number is not often controlled nor modeled when building damage models are implemented. (2) After the main event, it is common to expect several aftershocks, whose effects are often neglected in analytical models. Furthermore, in the case of empirical building damage models, the empirical observations include both the effects of the mainshock and the aftershocks occurred before the date of the field survey. Recall that building damage inventory is often performed after several days or even weeks. Despite these limitations, the fragility functions play an important role in seismic risk analysis.

The synthetic EBDS model developed in this paper is presented to support decision makers in taking appropriate preventive measures. This model is used to develop scenarios for performing further analysis, such as the evacuation of survivors and relief distribution for urban areas in Japan.

Acknowledgments

This research is supported by the Japan Science and Technology Agency (JST) (J150002645) through the SICORP project “Increasing Urban Resilience to Large Scale Disaster: The Development of a Dynamic Integrated Model for Disaster Management and Socio-Economic Analysis (DIM2SEA).” The building damage survey used in the case study was provided by Masumi Yamada. Futhermore, the anonymous reviewers, whose comments improved the quality of the article, are gratefully acknowledged.

References

[1] R. McGuire, Seismic hazard and risk analysis, Engineering monographs on miscellaneous earthquake engineering topics, Earthquake Engineering Research Institute, 2004.
[2] ATC, Earthquake Damage Evaluation Data for California. Report ATC-13, Applied Technology Council, Redwood City, CA., 1985.
[3] R.V. Whitman, J.W. Reed, S.-T. Hong, Earthquake damage probability matrices, In: Proceedings of the Fifth World Conference on Earthquake Engineering (1974) 2531–2540.
[4] F. Yamazaki, O. Murao, Vulnerability functions for Japanese buildings based on damage data from the 1995 Kobe earthquake, Vol. 2 of Implications of Recent Earthquakes on Seismic Risk, Imperial College Press, 2000.
[5] N. Yamaguchi, F. Yamazaki, Fragility curves for buildings in Japan based on damage surveys after the 1995 Kobe earthquake, in: Proceedings of the 12th World Conference on Earthquake Engineering, no. 2541, 2000, p. 8 pages.
[6] K. Horie, H. Hayashi, T. Okimura, S. Tanaka, N. Maki, N. Torii, Development of seismic risk assessment method reflecting building damage levels, fragility functions for complete collapse of wooden buildings, in: Proceedings of the 13th World Conference Earthquake Engineering, Vancouver, B.C., Canada, 2004, p. 15 pages.
[7] ATC, Seismic Evaluation and Retrofit of Concrete Buildings. Report ATC-40, Applied Technology Council, Redwood City, CA., 1996.
[8] BSSC, NEHRP guidelines for the seismic rehabilitation of buildings, NEHRP Guidelines for the Seismic Rehabilitation of Buildings, Building Seismic Safety Council (U.S.) and United States. Federal Emergency Management Agency and Applied Technology Council, 1997.
[9] C.A. Kircher, R.V. Whitman, W.T. Holmes, HAZUS Earthquake Loss Estimation Methods, Nat. Hazards Rev. 7 (2) (2006) 45–59.
[10] S.K. Ploeger, G.M. Atkinson, C. Samson, Applying the hazus-mh software tool to assess seismic risk in downtown ottawa, canada, Nat. Hazards 53 (1) (2010) 1–20, http://dx.doi.org/10.1007/s11069-009-9408-x.
[11] J.W.F. Remo, N. Pinter, Hazus-mh earthquake modeling in the central USA, Nat. Hazards 63 (2) (2012) 1055–1081, http://dx.doi.org/10.1007/s11069-012-0206-5.
[12] J. Moehle, G.G. Deierlein, A frameork methodology for performance-based earthquake engineering, in: Proceedings of the 13th World Conference Earthq. Eng., Vancouver, B.C., Canada, 2004, p. 13 pages.
[13] C.A. Goulet, C.B. Haselton, J. Mitrani-Reiser, J.L. Beck, G.G. Deierlein, K.A. Porter, J.P. Stewart, Evaluation of the seismic performance of a code-conforming reinforced-concrete frame building from seismic hazard to collapse safety and economic losses, Earthq. Eng. Struct. Dyn. 36 (13) (2007) 1973–1997, http://dx.doi.org/10.1002/eqe.694.
[14] K.M. Solberg, R.P. Dhakal, J.B. Mander, B.A. Bradley, Computational and rapid expected annual loss estimation methodologies for structures, Earthq. Eng. Struct. Dyn. 37 (1) (2008) 81–101, http://dx.doi.org/10.1002/eqe.746.
[15] T. Yang, 12 - assessing seismic risks for new and existing buildings using performance-based earthquake engineering (PBEE) methodology, in: S. Tesfamariam, K. Goda (Eds.), Handbook of Seismic Risk Analysis and Management of Civil Infrastructure Systems, Woodhead Publishing Series in Civil and Structural Engineering, Woodhead Publishing, 2013, pp. 307–333. http://dx.doi.org/10.1533/9780857098986.3.307.
[16] M. Shinozuka, M.Q. Feng, J. Lee, T. Naganuma, Statistical analysis of fragility curves, J. Eng. Mech. 126 (12) (2000) 1224–1231, http://dx.doi.org/10.1061/(ASCE)0733-9399(2000)126:12(1224).
[17] K. Porter, R. Kennedy, R. Bachman, Creating fragility functions for performance-based earthquake engineering, Earthq. Spectra 23 (2) (2007) 471–489.
[18] P.H. Galanis, J.P. Moehle, Development of collapse indicators for risk assessment of older-type reinforced concrete buildings, Earthq. Spectra 31 (4) (2015) 1991–2006, http://dx.doi.org/10.1193/080613EQS225M.
[19] E. Mas, A. Suppasri, F. Imamura, S. Koshimura, Agent-based simulation of the 2011 great east japan earthquake/tsunami evacuation: an integrated model of tsunami inundation and evacuation, J. Nat. Disaster 34 (1) (2012) 41–57, http://dx.doi.org/10.2328/jnds.34.41.
[20] E. Mas, S. Koshimura, F. Imamura, A. Suppasri, A. Muhari, B. Adriano, Recent advances in agent-based tsunami evacuation simulations: case studies in indonesia, thailand, japan and peru, Pure Appl. Geophys. 172 (12) (2015) 3409–3424, http://dx.doi.org/10.1007/s00024-015-1105-y.
[21] R. Das, S. Hanaoka, An agent-based model for resource allocation during relief distribution, J. Humanit. Logist. Supply Chain Manag. 4 (2) (2014) 265–285, http://dx.doi.org/10.1108/JHLSCM-07-2013-0023.
[22] A. Nejat, I. Damnjanovic, Agent-based modeling of behavioral housing recovery following disasters, Comput.-Aided Civil. Infrastruct. Eng. 27 (10) (2012) 748–763, http://dx.doi.org/10.1111/j.1467-8667.2012.00787.x (URL ⟨http://dx.doi.org/10.1111/j.1467-8667.2012.00787.x⟩).
[23] ESRI, ESRI Shapefile Technical Description, ESRI White Paper (1998) 34 http://dx.doi.org/10.1016/0167-9473(93)90138-J. URL ⟨http://www.esri.com/library/whitepapers/pdfs/shapefile.pdf⟩.
[24] S. Aoi, T. Kunugi, H. Fujiwara, Strong-motion seismograph network operated by nied: k-net and kik-net, J. Jpn. Assoc. Earthq. Eng. 4 (3) (2004) 65–74.
[25] M. Matsuoka, N. Yamamoto, Web-based Quick Estimation System of Strong Ground Motion Maps Using Engineering Geomorphologic Classification Map and Observed Seismic Records, in: Proceedings of the 15th World Conference Earthq. Eng. (2012) 10 pages.
[26] Bureau of Urban Development, Tokyo Metropolitan Government, Regional hazard level measurement survey report on earthquakes, ⟨http://www.toshiseibi.metro.tokyo.jp/bosai/chousa_6/home.htm⟩, [Online; (accessed 19 March 2018) (2018).
[27] T. Nagao, F. Yamazaki, Analysis of Building Damage in Kashiwazaki City due to the 2007 Niigata-Ken Chuetsu-Oki Earthquake, Proceedings of the Social Safety Science 15 (2011) 249-254 (In Japanese).
[28] K.A. Porter, Assembly-based vulnerability of buildings and its uses in seismic performance evaluation and risk-management decision-making, Stanford University, Stanford, CA (2000).
[29] Japan Meteorological Agency, The number of aftershocks of recent inland earthquakes in Japan, ⟨http://www.data.jma.go.jp/svd/eqev/data/2016_04_14_kumamoto/kaidan.pdf⟩, [Online; (accessed 07 August 2017) (2017).

[30] Cabinet Office of Japan, Summary of damage situation in the Kumamoto earthquake sequence, ⟨http://www.bousai.go.jp/updates/h280414jishin/index.html⟩, [Online; (accessed 07 August 2017) (2017).
[31] M. Yamada, J. Mori, H. Sakaue, T. Hayashida, M. Yamada, K. Hada, Y. Fujino, S. Fukatsu, E. Nishihara, T. Ouchi, A. Fujii, Investigation of the damage mechanism in the Mashiki-town for the 2016 Kumamoto earthquake: Part 1 building damage survey, Abstract of the Seismological Society Japan Fall Meeting.
[32] M. Yamada, J. Ohmura, H. Goto, Wooden building damage analysis in mashiki town for the 2016 kumamoto earthquakes on april 14 and 16, Earthq. Spectra 33 (4) (2017) 1555–1572, http://dx.doi.org/10.1193/090816EQS144M.
[33] Geospatial Information Authority of Japan, Maps and aerial photographs browsing service, ⟨http://maps.gsi.go.jp⟩, [Online; (accessed 08 August 2017) (2017).
[34] J.J. Bommer, J. Douglas, F. Scherbaum, F. Cotton, H. Bungum, D. Fah, On the selection of ground-motion prediction equations for seismic hazard analysis, Seismol. Res. Lett. 81 (5) (2010) 783, http://dx.doi.org/10.1785/gssrl.81.5.783.